Thermal Management of Compact Nanocrystalline Inductors for Power Dense Converters

Yiren Wang, Gerardo Calderon-Lopez and Andrew Forsyth
School of Electrical and Electronic Engineering
The University of Manchester
Manchester M13 9PL, UK
Email: {yiren.wang, gerardo.calderon-lopez, andrew.forsyth}@manchester.ac.uk

***Abstract*— Enhanced thermal management continues to be the key to the miniaturisation of high-frequency magnetic components and to increased converter power densities. Thermal finite element analysis has been used to examine the use of high-thermal-conductivity ceramic heat spreaders in the potted structure of a nanocrystalline-cored DC inductor to mitigate the local temperature rise due to the concentrated gap losses. The thermal performance of different heat spreader and potting materials has also been investigated. The heat spreader technique is validated by experimental results on two 350 A, 60 kHz DC inductors, showing a hot spot temperature reduction of 20 °C with embedded aluminium nitride heat spreaders, which may allow a smaller core to be used. By using the heat spreaders about 30 % weight reduction is illustrated for a higher frequency DC inductor design (300 A, 150 kHz). Furthermore, the impact of the potting compound's thermal conductivity is studied, revealing that a size reduction of up to 50% is possible with the heat spreaders in addition to an improved potting material.**

Keywords—thermal management; DC inductor; heat spreader; nanocrystalline core

I. INTRODUCTION

The miniaturisation of magnetic components is a perennial challenge for power electronics engineers. High-frequency magnetic components can account for more than 50 % of the weight of some converter systems [1], therefore, to achieve the increased power densities that are being demanded in some emerging applications, for example on-board electric vehicles and in the more-electric aircraft, highly compact magnetic components are essential.

Emerging wide bandgap devices using silicon carbide (SiC) or gallium nitride (GaN) are enabling increases in converter switching frequency, potentially leading to significant size and weight reductions of magnetic components. However, the downsizing of magnetic components is ultimately thermally limited [2], as the high frequency losses in the components tend to increase at higher frequencies and the surface area available for heat transfer is smaller from a reduced component size. This creates a need for improved thermal management within the magnetic components to ensure that hot spot temperatures remain within the limits of the materials, and this problem is particularly acute in some transport applications where the ambient temperatures can be high.

Nanocrystalline materials have a high saturation flux density of over 1 T and low specific hysteresis losses which are comparable with those in ferrites, offering the possibility of smaller wound components [1, 3]. These materials are manufactured as a thin metallic ribbon, approximately 18 μm thick, which may be used to build up finely-laminated cores, normally referred to as tape-wound cores. Due to the conductivity of the metallic ribbon, these cores are susceptible to gap losses whereby the air-gap fringe field can create eddy currents within the laminations and cause intense, localised heating around the edges of the gaps [4]. Without thermal management, the local hot spot may damage the insulation material between core laminations, and therefore the achievable size reduction at elevated operating frequencies may be limited.

Encapsulation using a thermally conductive epoxy has been commonly used for thermal management of magnetic components [5-9]. However, with highly localised losses the heat removal by encapsulation can be limited due to the relatively low thermal conductivity of potting materials, typically around 2 W/mK. In [10], heat transfer components made with highly thermally conductive materials or heat pipes are used to extract the heat from the magnetic component to an external heat sink. One of the disadvantages of this method is the added volume and weight. In addition, the heat transfer components or heat pipes are often metal-based. Eddy currents may be induced and cause additional losses, making them unsuitable for use around the air gaps. And when placed next to laminated cores, the heat pipes need to be electrically isolated, which may downgrade their heat transfer capabilities. It has been mentioned in the literature that ceramic materials may be used in the thermal management of magnetic components and compact power electronic modules [11, 12], but the effectiveness of ceramic heat spreaders has not been quantified, especially for the management of concentrated losses in laminated cores where the thermal conductivities are anisotropic.

This paper examines the use of ceramic heat spreaders for the thermal management of a compact tape-wound inductor with highly localised gap loss. The inductor uses a nanocrystalline Finemet C-core and copper foil winding which are encapsulated in an aluminium heat sink. With the help of

This work was supported by the U.K. Engineering and Physical Sciences Research Council (EPSRC) National Centre for Power Electronics within the Components Theme [EP/K034804/1] and also by a feasibility study grant from the EPSRC Challenge Network in Automotive Power Electronics.

finite element analysis (FEA) of the gapped inductor, the loss distributions are identified. The high-thermal-conductivity heat spreaders are placed at the predicted local hot spots as a simple, but effective technique to reduce significantly the hot spot temperatures without requiring additional space or assembly effort. 3D FEA thermal modelling of the inductor is presented, showing that the heat spreader technique is particularly effective for localised losses, whilst for uniformly distributed losses their benefits are less significant. Experimental results are provided for validation from two 350 A, 60 kHz prototype inductors, showing a 20 °C reduction at the hot spot with the use of heat spreaders. The design and temperature performance of the heat spreader and potting materials is explained using thermal FEA for five inductors which are intended for a 75 kHz, 60 kW interleaved SiC DC-DC converter. It is shown that the heat spreader technique has the potential to reduce the inductor weight by about 30 % without exceeding the core's thermal limit, and with a better thermal potting material, a further weight reduction of 20 % may be achieved.

II. DC Inductor Topology and Prototype Design

To maintain the air gap length in the inductor cores, plastic shims or other insulating materials are commonly used as gap spacers, but the thermal conductivity of these materials is usually poor. Furthermore, the core laminations tend to prevent the heat flow from the edges of the gaps to the centre of the core. Therefore, to manage the local heating due to the gap loss around the core edges, aluminium nitride (AlN) heat spreaders were used within the air gaps to replace the gap spacers, without additional space requirement or assembly effort. The inductor was then encapsulated in an aluminium can with thermally conductive potting material, Fig.1. The encapsulation also provides mechanical robustness to the whole structure. The potted inductor will be mounted to the converter's main cold plate or heat sink.

The AlN heat spreaders are not electrically conductive, but have a high isotropic thermal conductivity of 92 W/mK. The thickness of the heat spreaders will form the required air gap length. They will enable the heat to flow easily from the core edges and across the core cross-sectional area, then through the core to the can. The dimensions of the spreaders were chosen to occupy all the inner area available inside the coils, slightly larger than the core cross-section, as seen in Fig. 1, and this will also enhance the heat flow into the surrounding potting material and the winding.

To illustrate the concept, a 5.1 µH, 350 A, 60 kHz DC inductor was considered, which was taken from a 25 kW, dual-interleaved DC-DC converter within an electric vehicle power train. The inductor used a set of F3CC0032 Finemet cut cores from Hitachi Metals [13] with copper foil windings. A total air gap length, l_g, of 4.4 mm was used to avoid saturation under high DC currents. The winding was wound with six turns of 0.8 mm thick and 51 mm wide copper foil, and was split into two coils around each core leg. The coils were spaced away from the core by a minimum of 2.2 mm, half the total gap length, to minimise the additional copper losses caused by the air-gap fringe field. To examine the benefits of the heat spreaders, a separate inductor without heat spreaders was also constructed with the same electrical, magnetic and mechanical

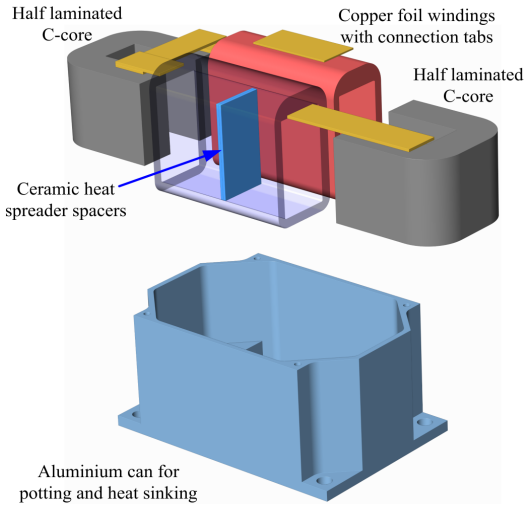

Fig. 1. Exploded drawing of the inductor assembly with the ceramic heat spreaders.

specifications, the only difference being glass reinforced plastic (GRP) shims were used as air gap spacers instead.

III. Finite Element Modelling

3D finite element thermal models have been used to estimate the steady-state temperatures reached by the potted inductor and to examine the use of ceramic heat spreaders for temperature reduction. The simulations included the magnetic core, copper foil winding, GRP gap spacers/AlN heat spreaders and the encapsulation. The bottom face of the aluminium can was treated as a fixed temperature boundary condition, and the temperature is equal to the steady-state temperature of the converter's cold plate. All other outer surfaces of the potted component were defined as perfect insulators, and therefore all the heat was removed by conduction through the base of the can. The thermal model was solved in the Opera 3D FEA software [14] using the static thermal solver, TEMPO/ST.

A. Material Thermal Properties

The laminated core was modelled as homogeneous blocks with anisotropic thermal characteristics in the thermal simulation. The thermal conductivities used for the core were 10 W/mK along the laminations and 0.5 W/mK through the laminations to take into account the poor heat transfer caused by the insulation between laminations [11].

The foil wound coils with Kapton insulation between the turns also comprise a layered structure similar to the laminated core. They were also modelled as homogeneous blocks, with equivalent anisotropic thermal conductivities along the turns and through the turns. Each coil has three turns of 0.8 mm copper foil and the measured total winding thickness, t_{coil}, is around 4.5 mm. In addition to the insulation film (0.13 mm thick), the gaps between the turns, filled with potting material, resulting in a poor heat flow through the turns. The equivalent thermal characteristics of the coils were estimated from the weighted average thermal conductivities of copper, k_{cu}, insulation film, k_{in}, and potting material, k_{pot}, as in (1) and (2) [15], where t_{cu}, t_{in}, and t_{pot} are the thicknesses of copper foil, insulation film and gaps between turns, respectively. Table I

summarises the thermal conductivities of the different materials used in the model.

$$k_{along} = \left(k_{Cu}t_{Cu} + k_{in}t_{in} + k_{pot}t_{pot}\right)/t_{coil} \quad (1)$$

$$k_{through} = t_{coil}/\left(t_{Cu}/k_{Cu} + t_{in}/k_{in} + t_{pot}/k_{pot}\right) \quad (2)$$

TABLE I. MATERIAL PROPERTIES USED IN THERMAL FEA

Model Element	Thermal Conductivity (W/mK)
Aluminium Can	180
Potting material	1.8
Insulation	0.12
Finemet core - along laminations - through laminations	 10 0.5
Foil winding - along turns - through turns	 206 0.8
AlN heat spreader	92
GRP gap spacers	0.35

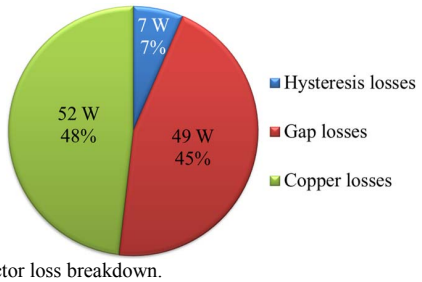

Fig. 2. Inductor loss breakdown.

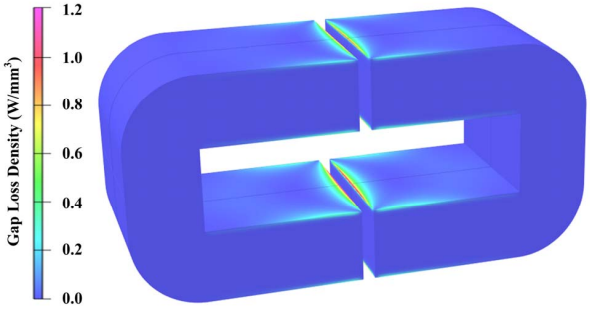

Fig. 3. Gap loss density distribution in the core (part number: F3CC0032, l_g = 4.4 mm, B_m = 0.16 T, 60 kHz).

B. Inductor Losses

The loss mechanisms in the inductor prototype comprise three parts: copper losses, hysteresis loss and gap loss. Fig. 2 shows the loss breakdown in the inductor operating with a peak to peak current ripple, ΔI_L, of 130 A at 60 kHz and a DC current, I_{dc}, of 160 A. The peak AC flux density, B_m, is 0.16 T.

The copper losses, including the DC and AC loss components, were calculated from the published loss equations in [16, 17], and the hysteresis loss was measured using the B-H loop method on the same core without air gaps. The gap loss was predicted from a separate electromagnetic FEA simulation [4], and the loss density distribution is shown in Fig. 3. The gap loss contributes around half of the total loss, which is not uncommon in compact, high-frequency DC inductors with nanocrystalline cores, and it is highly concentrated around the gap edges of the core, which will lead to local hot spots.

C. Modelling of Localised Loss Density

The hysteresis loss and copper losses were assumed to be evenly distributed throughout the core and coil volumes, whilst the gap loss is highly concentrated. To account for the non-uniform gap loss distributions, two methods were considered.

The first method couples the thermal analysis with the electromagnetic one by directly importing the loss density, Fig. 3, from the electromagnetic analysis. Whilst the electromagnetic model only includes the core, ideal conductors and air, the thermal model has additional geometric volumes for the encapsulation. The loss density is transferred between the two analyses via a table file based on the finite element mesh. This method provides the most accurate loss information to the thermal analysis. However, as the electromagnetic analysis requires a fine mesh for accurate eddy current calculation at high frequency (0.3 mm mesh used for Fig. 3), the thermal model needs at least to match this mesh size to capture the variation of the loss density. This will result in a large model and table files, and it is time consuming to write and load data between analyses and also to solve the models.

The second method models the localised loss distribution in the core with lumped blocks, assuming uniform loss in each block, as shown in Fig. 4. This method allows the thermal model to be solved independently with a coarser mesh so that the simulation time is significantly reduced. To approximate the gap loss distribution shown in Fig. 3, the surface regions of the core limbs were divided into four sections, Fig. 4(a), and they are: the core gap edges, marked as Gap_Out and Gap_In for the outer surface and inner surface, respectively; the core side edges, Side_Out and Side_In; and then the rest of the surface was divided into two regions: Out1 and Out2, In1 and In2. The middle of the core limbs, MidCore, was treated as a single block where the gap loss density is minimum.

The dimensions of the surface blocks, labelled in Fig. 4(b), were determined from the loss density distribution from the electromagnetic solution. For the operating point shown in Fig. 3, the depth of the surface regions, d, was 1 mm, and the dimensions of blocks, L_{Gout}, L_{Gin}, and L_{Side}, were chosen to be 1 mm, 1.2 mm, and 1 mm, respectively. At these distances, the loss densities drop to 33% of their peak values at the core gap and side edges. $L_{SideOut}$ and L_{SideIn} were selected as 10 mm and 15 mm, respectively. About 70% of the losses along the core side edges are contained within these regions. The peak loss density occurring at the centre of the gap edges increases when the gap length, frequency, flux density or core width increases [4]. However, the loss distribution does not change noticeably with the frequency or the flux density; therefore, the same block dimensions can be used for a specific component at different operating conditions, as shown later in Section IV. Nevertheless as the gap length becomes smaller or the core strip becomes narrower, the loss density concentrates more towards the gap edges. This results from a more concentrated

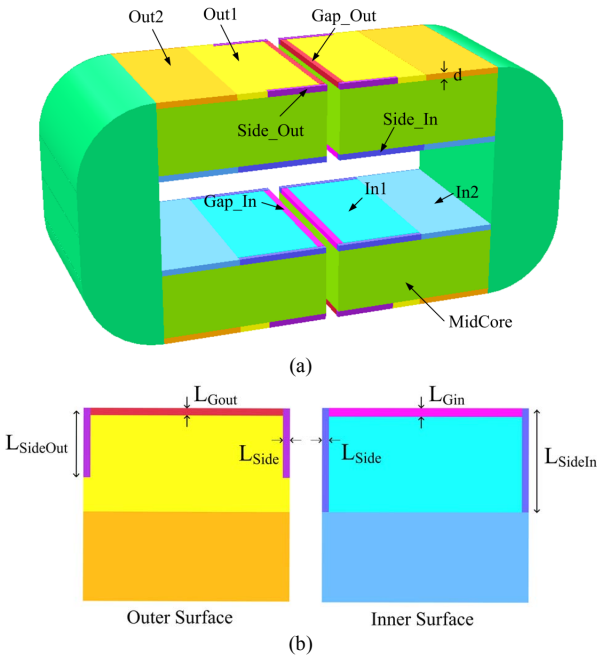

Fig. 4. Lumped blocks for gap loss distribution in the core.

fringing flux around smaller air gaps and reduced eddy current loops due to narrower core lamination width. Smaller blocks are then needed to approximate the loss distribution. Therefore, the choice of the dimensions of the loss distribution blocks depends on the inductor's physical design parameters only. The losses occurring in the lumped blocks were then calculated individually from the electromagnetic analysis through volume integration. The approximated allocations of the gap loss in these blocks are listed in Table II. The outer core surface regions contribute around 37% of the total gap loss, whilst around 58% of the gap loss occurs in the inner surfaces. About 45% of the gap loss is concentrated around the gap edges, and 15% of the loss is distributed along the side edges of the core. Based on the modelling of the F3CC0032 core, it has been found that the percentage loss in the blocks is independent of operating conditions for gap lengths from 2 to 6 mm. The mesh size used for the block model was 1 mm, matching the minimum dimension in the model.

TABLE II. GAP LOSS ALLOCATION IN BLOCK MODEL (PART NUMBER: F3CC0032, l_g = 4.4 mm).

Block name		Percentage of total gap loss
Outer surface regions	Gap_Out	17.7 %
	Side_Out	6.0 %
	Out1	8.0 %
	Out2	4.8 %
Inner surface regions	Gap_In	26.5 %
	Side_In	8.6 %
	In1	11.7 %
	In2	10.7 %
MidCore		6.0 %

Comparing with the coupled FEA method, the size of the block FEA model was reduced by around 90 % with a coarser mesh, and the overall modelling time was reduced by more than 75 %.

D. Simulation Results

Fig. 5 shows simulation results of the predicted steady-state temperature rise, ΔT, in the core using the coupled thermal analysis, and Fig. 6 shows the results using the block approximation method. The core surfaces facing out of the page in Figs. 5 and 6 are hotter than the surfaces facing into the page as these surfaces are at the top of the aluminium can when potted. The inner core surfaces are slightly hotter than the outer surfaces. The hot spot from the coupled analysis is at the centre of the gap edges, on the core surfaces, while the simulation using the block method estimates a hot spot slightly inside the core. This is because the gap loss is concentrated towards the surface, but the block model uses uniform volume heat sources to represent it. However, both simulations show similar hot spot temperature rises above the heat sink. Furthermore, the hot spot temperatures are reduced by around 20 °C and the core temperature becomes more uniform with the use of AlN heat spreaders.

It is clearly evident that the heat spreaders are effective in reducing the hot spot temperature with significant localised loss conditions. However, without the presence of localised losses the temperature distribution in the component tends to be more uniform, and the usefulness of the heat spreaders may be reduced. Fig. 7 shows the simulated temperatures in the core assuming the gap loss is evenly distributed in the core. Comparing to the results shown in Figs. 5 and 6, the total loss in the inductors is the same; however the simulated maximum temperature is around 15 °C lower in the core without heat spreader. With a uniform loss distribution, the temperature distribution in the component tends to be more uniform and the core does not have a local hot spot. However, with the AlN

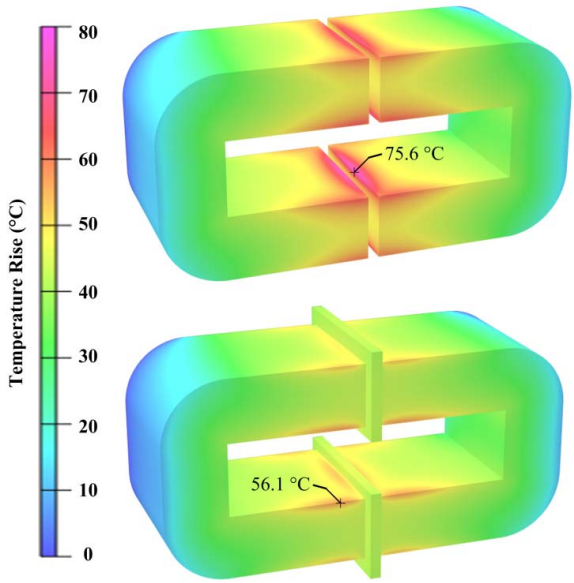

Fig. 5. Thermal FEA results using the coupled analysis, showing the core temperature rise above the heat sink. Top: core without heat spreader (GRP spacers); bottom: core with AlN heat spreaders.

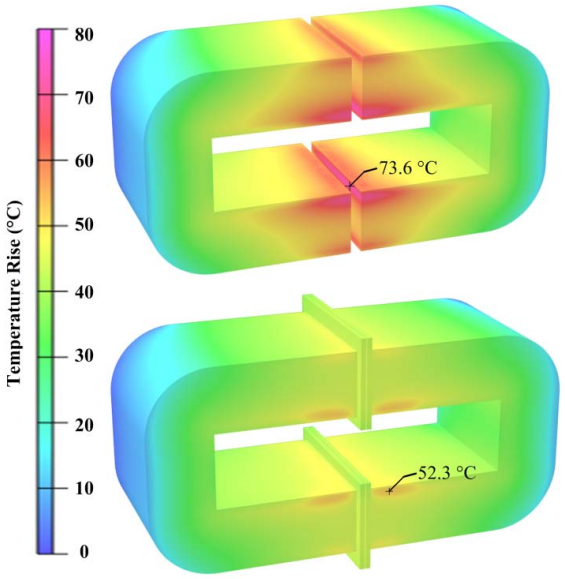

Fig. 6. Thermal FEA results using the block approximation method, showing the core temperature rise above the heat sink. Top: core without heat spreader (GRP spacers); bottom: core with AlN heat spreaders.

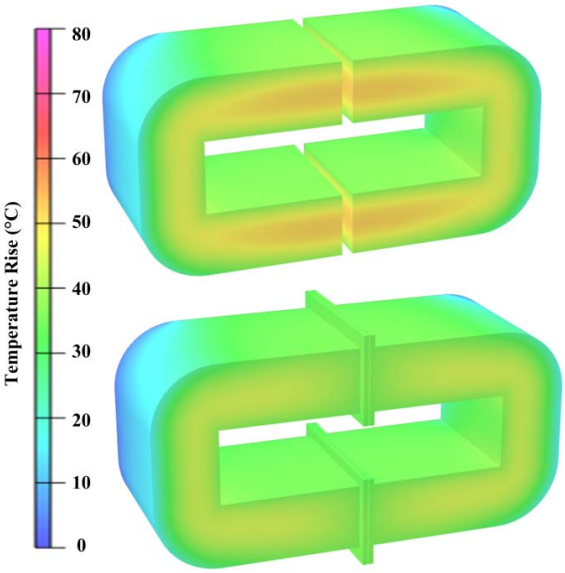

Fig. 7. Thermal FEA result assuming uniform gap loss distribution in the core showing temperature rise above the heat sink. Top: core without heat spreader (GRP spacers); bottom: core with AlN heat spreaders.

heat spreaders the core temperature is reduced further by 7 °C, much less than the 20 °C reduction when the losses are concentrated.

IV. Experimental Validation

The heat spreader technique has been experimentally validated by temperature measurements on the prototype inductors. To examine the temperature distribution in the inductor, several temperature sensors were fixed to different locations on the core before potting, especially around the gaps, as shown in Fig. 8, to identify the hot spots within the component. The predicted and measured steady-state temperature rise in the prototypes without and with the heat spreaders are compared in Fig. 9. The hot spot temperature was reduced by 20 °C as predicted, and a temperature reduction was observed at all monitored locations, especially around the gaps.

To provide further validation of the FE thermal model, the predicted and measured temperatures are compared under a different operating condition, Fig. 10. With a DC current of 145 A and a peak to peak ripple of 80 A, the hysteresis loss, gap loss and copper loss are 4 W, 25 W and 26 W, respectively. The simulation and measurements still show excellent agreement, and the heat spreader reduces the hot-spot temperature, but due to the reduced power the reduction is now around 5 °C.

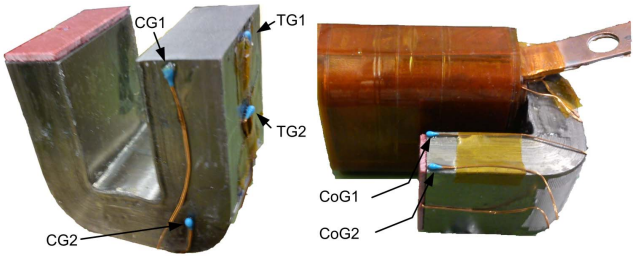

Fig. 8. Location of temperature sensors.

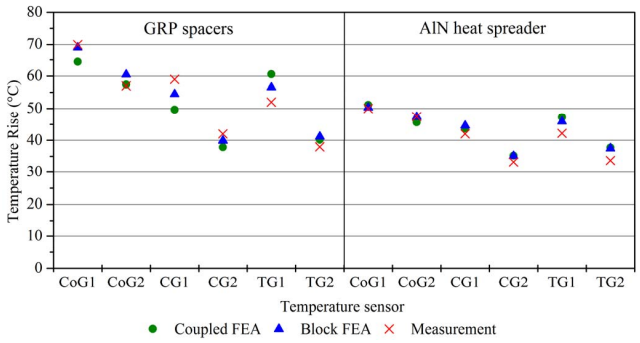

Fig. 9. FEA and measured steady-state temperature rise in the inductors without heat spreaders (GRP spacers) and with AlN heat spreaders (Inductor operating condition: I_{dc} = 160 A, ΔI_L = 130 A at 60 kHz, B_m = 0.16 T).

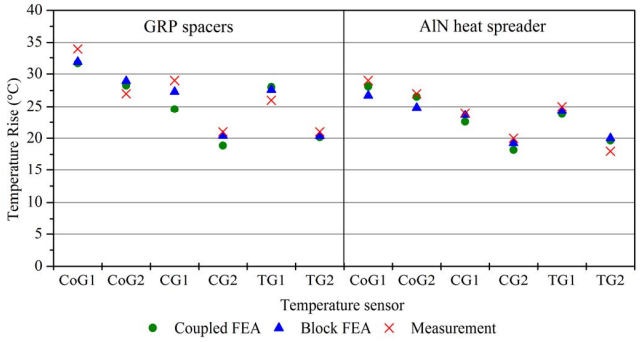

Fig. 10. FEA and measured steady-state temperature rise in the inductors without heat spreaders (GRP spacers) and with AlN heat spreaders. (Inductor operating condition: I_{dc} = 145 A, ΔI_L = 80 A at 60 kHz, B_m = 0.11 T).

V. Performance Evaluation of Potting and Heat Spreader Materials

The thermal FEA has been shown in Section IV to provide accurate estimations of temperatures in the encapsulated inductors. FE simulations were then used to evaluate the temperature reduction performance of different potting and heat spreader materials in the encapsulated DC inductors. The inductor considered here has the same topology as shown in Fig. 1, however, a smaller core (F3CC0016A [13]) was used and the component was designed for operation at a higher frequency, 150 kHz. This is an example of a high-frequency, reduced size magnetic component enabled by the use of SiC devices, where effective thermal management is vital to keep the core below its maximum operating temperature. The hysteresis loss used in the simulations was 33 W, the gap loss was 85 W and the copper loss was 56 W.

Fig. 11 shows the hot spot temperature in the core when different potting and heat spreader materials are used in the encapsulated structure. For the heat spreader materials, diamond, boron nitride, aluminium nitride, alumina, and a material equivalent to the potting compound are considered and compared against the GRP gap spacers. These materials are good thermal conductors as well as electrical insulators. In addition, the hardness of these materials provides enough mechanical strength between gaps to maintain the required air gap length. Whereas for the potting compound, materials with thermal conductivities up to 3.2 W/mK are currently available on the market, and 4 W/mK will be available soon [19]. Hypothetical values of 5 W/mK and 10 W/mK are also considered in the simulations to study the impact of the potting material on the thermal management for enabling future weight and size reductions.

In all cases, heat spreaders significantly reduce the hot spot temperature. However, the material of the heat spreaders appears to have little impact on the temperature reduction as long as the thermal conductivity is considerably higher than the thermal conductivity of the core or the potting compound. For example, when a potting material of 1 W/mK is used for encapsulation, the performance of diamond, with a thermal conductivity of 2000 W/mK, or aluminium nitride, 92 W/mK, do not appear to be significantly superior to alumina, 25 W/mK. However, a single tile of 100×100 mm, 1-mm thick aluminium nitride costs £ 562, whilst an alumina tile of the same dimensions costs £ 219 [18]. Furthermore, using a better potting material without heat spreaders may achieve the same temperature reduction benefit as the heat spreaders with poor potting material. For example, if a 10 W/mK potting material were available, the heat spreaders are no longer necessary, but still a smaller core could be used with heat spreaders.

Although there are several materials with good thermal conductivities available in the market, the selection of cheaper alternative materials to form the heat spreaders is limited because of their electrical or mechanical properties. Several options are derived from graphite so they are electrical conductive, whilst others are tacky or soft, making them unsuitable for holding the gaps between the half-cores. On the other hand, the majority of thermally conductive composites have anisotropic thermal properties and good electrical conductivity.

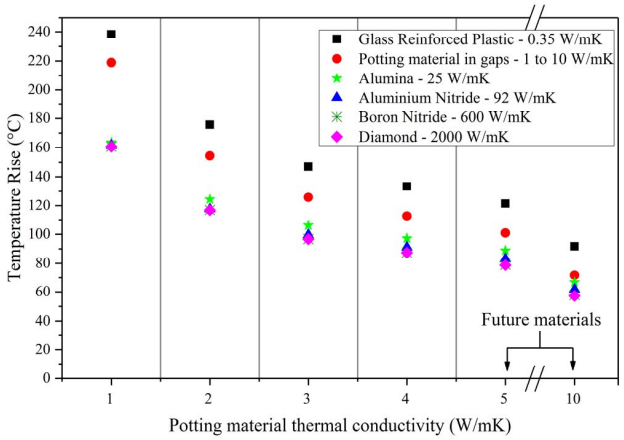

Fig. 11. Predicted temperature rise in the encapsulated inductor using different potting and heat spreader materials.

VI. Potential Weight Reduction with Different Thermal Management

By reducing the hot spot temperature, the heat spreaders may be used to reduce the size of an inductor by enabling the use of a smaller core. To demonstrate this, five inductors were designed for a 75 kHz, 60 kW dual-interleaved SiC DC-DC converter (the inductor operates with 150 kHz ripple due to interleaving). Design 1 considers free air convection, and all other designs are encapsulated, but with different materials for potting and heat spreading around the air gaps. The inductors have different parameters because they are optimised for minimum weight with different thermal arrangements, ensuring the cores operate within their thermal limits (155°C) under a transient overload condition of 90 kW at a DC current of 300 A and a cold plate or ambient temperature of 60 °C. The designs are summarised in Table III with the hot spot temperature estimated by thermal FEA, and the estimated weights and volumes of the designs are compared in Fig. 12. The minimum weight design has lower inductance and a higher ripple current, which will slightly increase the losses in the converter and may require additional capacitance for filtering. However, the capacitors in the converters only contribute around 8 % of the weight, while the magnetics are responsible for more than 50 % [1]. Therefore, the overall converter power density can be increased with a reduced size inductor, even at the cost of a slightly increased capacitor size.

Design 1 assumes free air convection and a big core has to be used. By comparing design 1 and design 2, it is shown that encapsulation –even with a relatively poor potting material of 1 W/mK, enables a significant volume reduction of 26 %. The weight reduction is less, only 9 %, due to the additional weight of the aluminium can and potting compound. Design 3, with an improved potting material of 2.1 W/mK, allows a further size and weight reduction of around 15 %. Design 3 and 4 use the same potting material, and the use of AlN heat spreaders contributes to a weight and volume reduction of the

encapsulated structure of 29.4 % and 12.2 % respectively. Furthermore with the highest performance potting material on the market, design 5, a further weight and volume reduction of 33.3 % and 16.7 % can be achieved. Overall, thermal management using heat spreaders together with improved encapsulations may achieve over 60 % reduction in size and over 50 % weight reduction compared with free air cooling, even though the losses are more than doubled.

TABLE III. MINIMUM WEIGHT INDUCTOR DESIGNS FOR FILTERING INDUCTOR FOR A 300 V – 750 V, 75 kHz, 60 kW DC-DC CONVERTER (COLD PLATE/AMBIENT TEMPERATURE: 60 °C).

Parameter	Design Number				
	1	*2*	*3*	*4*	*5*
Core part number [13]	F3CC-0125	F3CC-0063	F3CC-0040	F3CC-0032	F3CC-0016A
No. of turns	6	8	8	6	8
Gap length, mm	3.2	5.3	5.2	4	6.3
Inductance, µH	10.5	10.3	9.8	5.7	5.4
Heat spreader material	free air	GRP	GRP	AlN	AlN
Potting material, W/mK	free air	1	2.1	2.1	3.2
Total losses, W	111	151	172	206	243
Maximum ΔT at 90 kW transient, °C	95	95	93	96	97

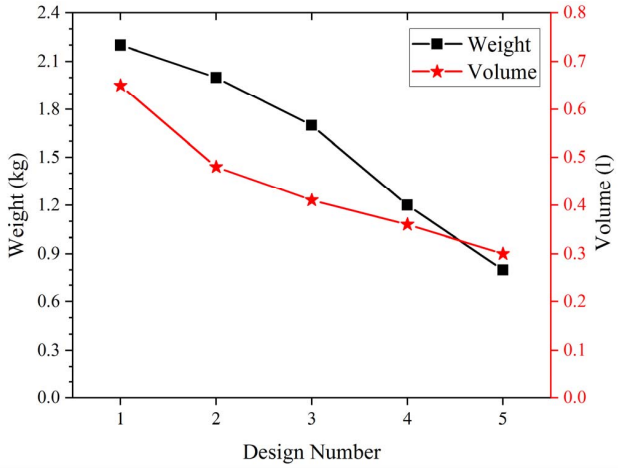

Fig. 12. Comparison of size and weight of optimised designs with different thermal management.

VII. CONCLUSIONS

Encapsulation is a commonly used technique to improve the heat transfer in magnetic components. However, finely laminated nanocrystalline cores often suffer from localised gap loss around the air gap regions, which requires additional heat paths to be created to avoid local overheating. This paper has presented the FE thermal modelling of a gapped inductor with localised gap loss and demonstrated the hot spot temperature reduction that may be achieved by using high-thermal-conductivity ceramic heat spreaders in the core gaps. The thermal performance of the inductors with and without the heat spreaders in the air gaps have been compared using FEA temperature predictions and validated experimentally, showing a significant temperature reduction at the gap areas which allows a smaller core to used.

Thermal FEA has also been used to evaluate the thermal performance of different heat spreader materials and potting materials for the encapsulation. The results suggest that the temperature reduction performance is independent of the heat spreader materials when the thermal conductivity of the heat spreaders is considerably higher than the core.

Furthermore, the potential size and weight reduction that can be achieved by the use of heat spreaders and improved encapsulation has been demonstrated. With the AlN heat spreaders, a 29.4 % weight reduction has been illustrated for a 300 A, 150 kHz inductor in a SiC DC-DC converter. A further reduction of 33.3 % may be achieved with a better encapsulation material.

REFERENCES

[1] G. Calderon-Lopez, A. J. Forsyth, D. L. Gordon and J. R. McIntosh, "Evaluation of SiC BJTs for high-power DC–DC converters," *IEEE Transaction on Power Electronics*, vol. 29, no. 5, pp. 2474-2481, May 2014.

[2] J. W. Kolar, D. Bortis, and D. Neumayr, "The ideal switch is not enough," in *2016 28th International Symposium on Power Semiconductor Devices and ICs (ISPSD)*, 2016, pp. 15-22.

[3] W. Yi, S. W. H. de Haan, and J. A. Ferreira, "High power density design of high-current DC-DC converter with high transient power," in *2010 IEEE Energy Conversion Congress and Exposition (ECCE)*, 2010, pp. 3001-3008.

[4] Y. Wang, G. Calderon-Lopez, and A. J. Forsyth, "High-frequency gap losses in nanocrystalline cores," *IEEE Transactions on Power Electronics,* vol. 32, pp. 4683-4690, 2017.

[5] R. Wrobel and P. H. Mellor, "Thermal design of high-energy-density wound components," *IEEE Transactions on Industrial Electronics,* vol. 58, pp. 4096-4104, 2011.

[6] M. Gerber, J. A. Ferreira, I. W. Hofsajer, and N. Seliger, "A high-density heat-sink-mounted inductor for automotive applications," *IEEE Transactions on Industry Applications,* vol. 40, pp. 1031-1038, 2004.

[7] M. Gerber, J. A. Ferreira, I. W. Hofsajer, and N. Seliger, "High density packaging of the passive components in an automotive DC/DC converter," *IEEE Transactions on Power Electronics,* vol. 20, pp. 268-275, 2005.

[8] Y. Bong-Gi, L. Byoung-Kuk, L. Sang-Won, J. Man-Chul, K. Jun-Hyung, and J. In-Bum, "Improvement of the thermal flow with potting structured inductor for high power density in 40kW DC-DC converter," in *IEEE Vehicle Power and Propulsion Conference (VPPC)*, 2012, pp. 1027-1032.

[9] J. Xue and F. Wang, "A practical liquid-cooling design method for magnetic components of EMI filter in high power motor drives," in *2016 IEEE Energy Conversion Congress and Exposition (ECCE)*, 2016, pp. 1-6.

[10] J. Biela and J. W. Kolar, "Cooling concepts for high power density magnetic devices," in *2007 Power Conversion Conference - Nagoya*, 2007, pp. 1-8.

[11] M. S. Rylko, B. J. Lyons, J. G. Hayes, and M. G. Egan, "Revised magnetics performance factors and experimental comparison of high-flux materials for high-current DC-DC inductors," *IEEE Transactions on Power Electronics,* vol. 26, pp. 2112-2126, 2011.

[12] J. Dirker, L. Wenduo, J. D. V. Wyk, A. G. Malan, and J. P. Meyer, "Embedded solid State heat extraction in integrated power electronic

modules," *IEEE Transactions on Power Electronics,* vol. 20, pp. 694-703, 2005.

[13] Hitachi Metals. (2016). *Metglas AMCC Series Cut Core/Finemet F3CC Series Cut Core. Catalog No. HJ-B11*. Available: http://www.hitachi-metals.co.jp/products/elec/tel/pdf/hj-b11.pdf

[14] Opera Simulation Software. Available: http://operafea.com

[15] S. Smith, *Magnetic Components. Design and Applications*. California: Van Nostrand Reinhold Company, 1985.

[16] N. Kondrath and M. K. Kazimierczuk, "Inductor winding loss owing to skin and proximity effects including harmonics in non-isolated pulse-width modulated dc-dc converters operating in continuous conduction mode," *Power Electronics, IET,* vol. 3, pp. 989-1000, 2010.

[17] M. S. Rylko, B. J. Lyons, K. J. Hartnett, J. G. Hayes, and M. G. Egan, "Magnetic material comparisons for high-current gapped and gapless foil wound inductors in high frequency DC-DC converters," in *Power Electronics and Motion Control Conference, 2008. EPE-PEMC 2008. 13th*, 2008, pp. 1249-1256.

[18] Goodfellow. (2017). Goodfellow Ceramics. Available: http://www.goodfellow-ceramics.com/

[19] LORD Corporation. *Thermoset TM SC-324 Thermally Conductive Silicone Encapsulant*. Available: https://www.lord.com/products-and-solutions/electronic-materials/thermoset-sc-324-thermally-conductive-silicone-